PHILOSOPHICAL MAGAZINE A, 2001, VOL. 81, NO. 5, 1143–1159

Deformation of copper single crystals to large strains at 4.2 K
II. Transmission electron microscopy observations of defect structure

M. NIEWCZAS†, Z. S. BASINSKI‡ and J. D. EMBURY

Department of Materials Science and Engineering, McMaster University, Hamilton, Ontario, Canada L8S 4L7

[*Received 17 February 2000 and accepted in revised form 20 June 2000*]

ABSTRACT

Transmission electron microscopy (TEM) observations of the dislocation substructure developed in high-purity single crystals of Cu deformed at 4.2 K have been carried out in order to relate the detailed defect structures to the mechanical and electrical properties discussed in part I. The results based on weak-beam TEM show that the dislocation substructure contains a very high density of narrow dislocation dipoles of vacancy character. These dipoles become progressively refined in scale as deformation continues. *In-situ* annealing experiments carried out in the transmission electron microscope allow the stability of these structures against annealing at room temperature and elevated temperatures to be studied. The observations suggest that fine dislocation dipoles can be annealed by processes such as pipe diffusion and that these defects represent the recoverable component of electrical resistivity. For comparison some studies were undertaken in Cu–5 at.% Ni single crystals which indicate that the recoverable component of resistivity in this alloy is smaller owing to the influence of the Ni on the pipe diffusion process. In addition, TEM studies indicate the complexity of processes occurring at the twin–parent interfaces produced in Cu deformed at 4.2 K. These interfaces have an important role in debris storage and in processes that can occur after large plastic strains at 4.2 K.

§1. INTRODUCTION

In part I (Niewczas *et al*. 2001) it was inferred from studies of plastic deformation of Cu crystals at 4.2 K that the large portion of the increase in electrical resistivity due to plastic flow can be removed by annealing below 250 K. This suggests that some types of defect can be removed by a process with a low activation energy such as pipe diffusion or the motion of some form of vacancy clusters. A basic difficulty in providing direct evidence of the defects involved in this process arises because the changes in electrical resistivity occur between 4.2 K and room tempera-

† Email: niewczas@mcmaster.ca

‡ Deceased 12 August, 1999. Professor Z. S. Basinski was instrumental in initiating this work and was involved in discussion of the results. However, he was not involved in the writing of this manuscript. It is the wish of his widow Ms S. J. Basinski that this note be included.

Philosophical Magazine A ISSN 0141–8610 print/ISSN 1460-6992 online © 2001 Taylor & Francis Ltd
http://www.tandf.co.uk/journals
DOI: 10.1080/01418610110033920

ture and thus all transmission electron microscopy (TEM) studies performed at room temperature are subsequent to changes in the defect structure.

The other important result in part I was that the twinning occurring at 4.2 K introduces large areas of twin–parent interfaces, which enforce compatible deformation in the twin and parent structures and influence defect accumulation and the final defect content in the crystal that can be achieved prior to failure.

In order to image both fine-scale defects and the structures in the vicinity of the interfaces, weak-beam imaging was used in the TEM studies. This method was developed by Cockayne *et al.* (1969) and was subsequently used by other researchers (for example Antonopoulos and Winter (1976) and Antonopoulos *et al.* (1976)) to study small-scale dislocation debris in fatigued Cu crystals.

The present work describes TEM studies which complement the investigations described in part I and extends these studies to include observations of the substructure developed in Cu–Ni alloy crystals during deformation at 4.2 K.

Thus the TEM observations are focused on the following:

(*a*) the evolution of the dislocation substructure,
(*b*) the analysis of small loop debris,
(*c*) the nature of twin–matrix interfaces and their role in the continued plastic flow;
(*d*) changes in dislocation debris due to annealing cycles at temperatures up to 573 K;
(*e*) comparison of the dislocation substructure in pure Cu with that in Cu–5 at.% Ni alloy.

§2. Experimental procedure

The evolution of the dislocation substructure of Cu and some Cu alloy single crystals with initial [541] orientation of the tensile axis was studied in various sections by means of TEM methods. Observations were carried out on samples deformed in tension at 4.2 K and after subsequent annealing, details of the annealing procedure and low temperature deformation have been described in part I (Niewczas *et al.* 2001).

From the deformed samples, slices about 0.5 mm thick were cut parallel to the given section by spark machining. Discs 3 mm in diameter were prepared from the slices. The trace of the relevant plane (direction) which allowed the identification of traces of other planes on the micrograph, was marked on each disc. To remove spark damage, discs were chemically polished from both sides down to a thickness of 300 μm in the solution described by Mitchell *et al.* (1967). Dimples about 200 μm in depth were subsequently made on one side of the discs using 80% phosphoric acid with a standard jet-polishing device. The final thinning was carried out in 80% phosphoric acid at room temperature, with an electropolishing rate of about 200 Å s^{-1}. Two-beam and weak-beam images of selected areas of the substructure were taken using low order reflections, usually $\pm\langle 111\rangle, \pm\langle 200\rangle$ or $\langle 220\rangle$ available in a given section.

Stereo pairs of micrographs were used for analysing the spatial arrangement of dislocation in three dimensions. The dislocation density was estimated by counting intersections of the dislocation line with a set of random circles as described by Steeds (1966). The relation $\rho = \pi N/2lt\ \mathrm{cm\,cm^{-3}}$ was used to calculate the dislocation density ρ, where N is a total number of intersections of projected circles with dis-

locations, l is a total circumference length and t is the foil thickness (Steeds 1966). The densities of dislocations obtained from two-beam and weak-beam micrographs were compared with dislocation density data deduced from resistivity measurements.

TEM observations were also carried out on undeformed (as-grown) samples, undeformed and annealed samples and also water quenched samples to study the initial structure in as-grown crystals and the effect of quenching and annealing on the initial structure. Thin foils were examined in Philips CM12STEM and JEOL 2010FEG electron microscopes.

The crystallographic notation adopted here is as follows: primary slip plane, $(11\bar{1})$; primary slip direction, [101]. The subscripts M and T refer to the parent and twin lattices respectively.

§ 3. Results

The results are reported in three sections. In § 3.1 the structure of crystals prior to deformation is dealt with. The dislocation substructure developed during deformation at 4.2 K in copper is presented in § 3.2. In § 3.3 the stability of this substructure at elevated temperatures is discussed and the dislocation substructure of Cu is compared with that of Cu–5 at.% Ni alloy. Figure 1 shows the tensile curves of Cu–5 at.% Ni and Cu single crystals deformed at 4.2 K, the substructures of which were studied by TEM.

3.1. *The structure of crystals prior to deformation*

The internal structure of as-grown Cu single crystals contains some curved dislocations and a number of small features, which were identified as small vacancy

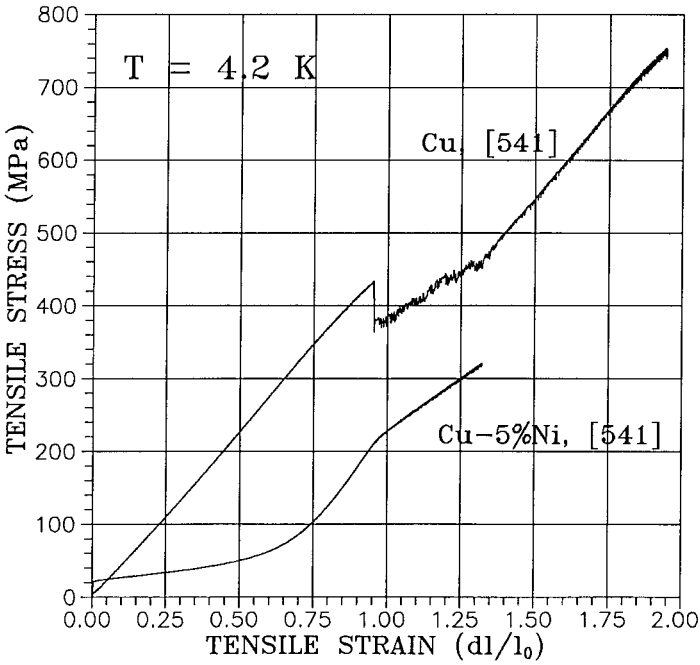

Figure 1. The tensile stress–strain curves for a Cu single crystal and Cu–5 at.% Ni deformed at 4.2 K.

clusters, as shown by arrowheads in the weak-beam micrograph in figure 2 (*a*). These clusters were randomly distributed on {111} planes; dislocations present in as-grown crystals were often decorated by vacancy precipitations as visible in figure 2 (*a*). As-grown crystals were subsequently annealed at a temperature of 1273 K for 72 h; some samples were water quenched and some were slowly cooled to room temperature and examined by TEM.

The internal structure of quenched samples is shown in figures 2 (*b*) and (*c*). Two types of defect introduced by water quenching were observed in the substructure: small vacancy clusters similar to those found in as-grown crystals, shown by arrowheads in figure 2 (*b*); and prismatic dislocation loops, typical effects of condensation of vacancies from supersaturated solution, shown by arrowheads in figure 2 (*c*).

In contrast with the substructure of the quenched samples, the internal structure of crystals slowly cooled to room temperature was free of vacancy clusters, as shown

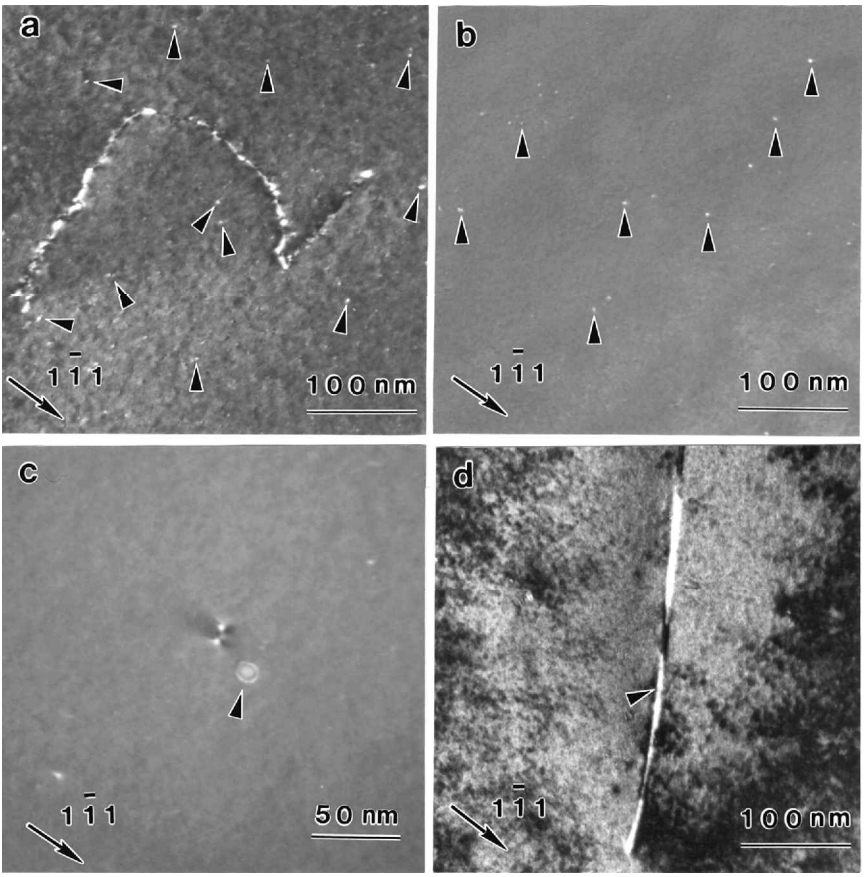

Figure 2. The internal structure of Cu crystals prior to deformation: (*a*) the structure of as-grown crystal with vacancy clusters (indicated by arrowheads) and jogged dislocation; (*b*), (*c*) the structure of the water-quenched crystal, where the vacancy clusters and quenched dislocation loops are indicated by arrowheads in (*b*) and (*c*) respectively; (*d*) the structure of the Cu crystal annealed at 1273 K followed by slow cooling to room temperature. Note that there is no evidence of vacancy precipitation in grown crystals followed by slow cooling.

in figure 2 (*d*). In order to eliminate the influence of defects due to quenched-in vacancies, all crystals were annealed at 1273 K followed by slow cooling to room temperature prior to deformation in tension at 4.2 K (Niewczas *et al*. 2001).

3.2. *Substructure in deformed crystals*

It was reported in part I (Niewczas *et al*. 2001) that the deformation process of Cu single crystals with [541] initial orientation of the tensile axis at 4.2 K, can be divided into three separate regions which were labelled A, B and C. In region A, the deformation proceeds predominantly by slip on the primary glide system $(11\bar{1})[101]_M$. In region B the deformation proceeds by twinning on the conjugate $(1\bar{1}1)[121]_M$ twinning system and results in conversion of about 70% of the sample into a twin-related orientation. Further deformation in region C proceeds by compatible slip in both the twinned and the untwinned part of the crystal. The dislocation substructure characteristic for each of those regions is presented below.

3.2.1. *Substructure in region A*

Examples of the dislocation substructure developed just before the onset of twinning at 4.2 K are shown in figure 3 and 4. Observations of the foil in the section parallel to the $(1\bar{1}\bar{1})_M$ cross-plane of the parent crystal demonstrates a well developed cell structure at this stage of the deformation, as shown in figure 3. The cell interior is bounded by layers of primary dislocations roughly parallel to the primary glide plane and layers of secondary dislocations in the non-coplanar conjugate plane. The average cell diameter is of the order of 0.3–0.4 μm (figure 3). Dislocations constituting the wall come mainly from the slip systems activated in the primary and conjugate slip planes, but short Lomer–Cottrell barriers (shown by arrowheads in figure 3(c)) were also found in the wall. Additionally, weak-beam analysis of the wall structure reveals a high density of the fine faulted loops produced by the primary system $(11\bar{1})[101]_M$; some are shown by arrowheads in figure 4. Detailed analysis of these defects, to be published elsewhere, shows that they are narrow faulted dipoles of vacancy type in the Z configuration. The overall dislocation density is higher in the wall by a factor of at least ten than in the cell interior.

3.2.2. *Substructure in region B*

Twinning converts the dislocation substructure of the parent crystal into a new configuration (Basinski *et al*. 1997). Figure 5 shows the substructure inside the twinned crystal observed under weak-beam diffracting conditions in $\mathbf{g} = [0\bar{2}0]$ operating reflection. A dislocation with Burgers vector $(a/2)[0\bar{2}0]$, which was transformed from a primary $(a/2)[101]$ dislocation is shown at Q. A high density of short dot-like faulted dipoles transformed from the faulted dipoles of the matrix is visible in the substructure. The length of these dipoles varies from dot-like defects to dipoles about 30–40 nm in length; some longer faulted dipoles are shown by arrowheads in figure 5. Overall, the dislocation substructure of the twinned crystal is much more refined than the substructure observed prior to twinning.

After the completion of twinning, some 30% of the crystal remains untwinned; thus the structure becomes a composite consisting of layers of twin and layers of matrix as was shown in figures 2 and (*b*) in part I (Niewczas *et al*. 2001).

3.2.3. *Substructure in region C*

Twinning deformation introduces a large number of twin–matrix interfaces. Based on the dark-field TEM observations the areal density of the matrix–twin interfaces in the foil at the beginning of region C was determined to be of the order of $10^7\,m^2\,m^{-3}$. These interfaces are effective obstacles for the dislocations activated in both the parent and the twin regions. In the early stage C, more than 95% of the matrix–twin boundaries are of $\Sigma = 3$ type as shown in figure 6(*a*). During subsequent deformation, additional rotations are produced owing to the accumulation of dislocations at the interfaces, as shown in figure 6(*b*).

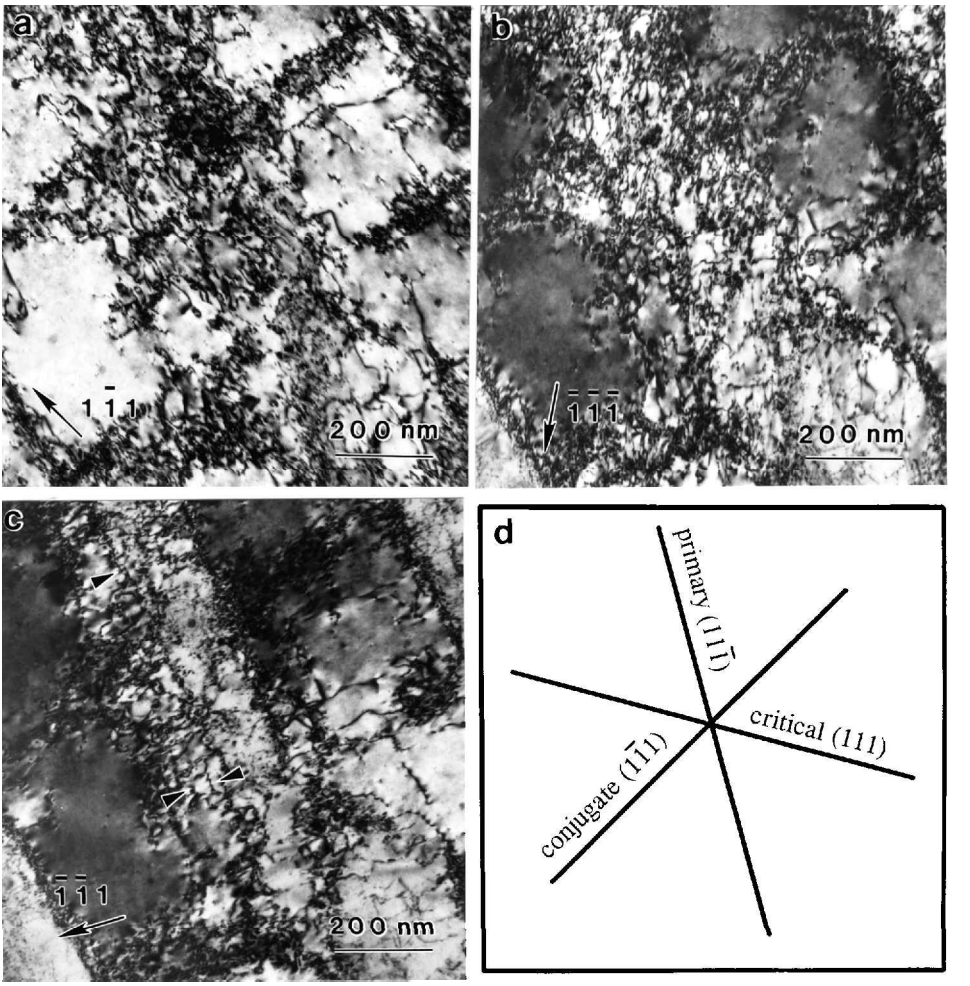

Figure 3. The bright-field two-beam observations of the dislocation substructure in the section parallel to the cross-glide plane in a Cu crystal deformed up to twinning at 4.2 K (end of region A): (*a*) (*b*) the micrographs show the development of the cell structure and the dislocation content in the wall; (*c*) primary dislocations with an $(a/2)[101]$ Burgers vector are out of contrast in the $\mathbf{g} = [\bar{1}\bar{1}1]$ reflection, and the $(a/2)[01\bar{1}]$ Lomer barriers are indicated by arrowheads; (*d*) Traces of {111} planes on the observation plane. Note that dislocation layers developed in the primary glide plane are rotated about 10° from the exact crystallographic position of this plane.

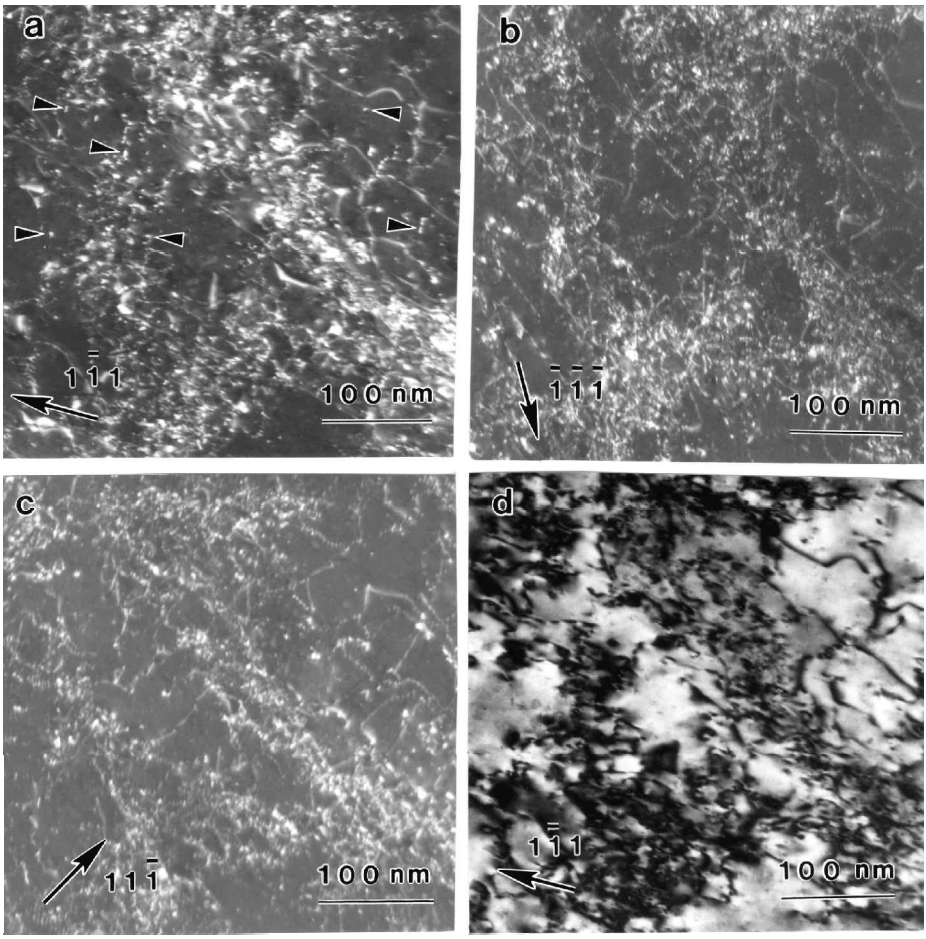

Figure 4. (*a*)–(*c*) Weak-beam observations of the defect content of the wall, in the section parallel to the cross-glide plane in the Cu crystal deformed up to twinning at 4.2 K (end of region A). Fine dot-like defects indicated by arrowheads in (*a*) are faulted dipoles formed by the transformation of narrow primary dipoles. Apart from the primary dislocations and primary debris the structure of the wall consists of a high density of secondary dislocations and small loops visible in $\mathbf{g} = [11\bar{1}]$ reflection in (*c*). (*d*) Two-beam observations of the same area for comparison.

The two regions, parent and twin, each develop a characteristic dislocation substructure, during compatible co-deformation in region C. After the onset of twinning the untransformed parent phase is oriented for slip in the conjugate slip system $(1\bar{1}1)[110]_M$ and critical slip system $(111)[1\bar{1}0]_M$ (Niewczas *et al.* 2001). The primary dislocations accumulated during stage A of the deformation are in essence forest dislocations with respect to the dislocations active in this stage; thus, further deformation involves intensive refinement of the pre-existing substructure by cutting. The dislocations activated in the critical $(111)_M$ and conjugate $(1\bar{1}1)_M$ planes are accumulated in the complicated three-dimensional dislocation network, as well as at the matrix–twin interfaces, leading to the observed increase in the work-hardening rate at this stage of deformation.

Figure 5. Weak-beam observation of the dislocation substructure inside the twin after region B. A dislocation with Burgers vector $(a/2)[0\bar{2}0]$ which is transformed from the primary $(a/2)[101]$ dislocation by twinning is shown at Q. The nanoscale dot-like defects indicated by arrowheads are faulted dipoles, transformed from faulted dipoles present in the parent crystal prior to twinning.

In order to obtain qualitative information about the types of defect produced in region C inside the twin, one has to account for defects inherited from the dislocation substructure of the parent crystal and for the new debris produced during subsequent deformation. The dislocation substructure inherited from the matrix becomes a strong obstacle for the new dislocations activated inside the twin. The deformation process involves intensive accumulation of defects in the entire volume of the twin, as well as at the matrix–twin interfaces. Figure 7 shows an example of the dislocation structure developed inside the twinned crystal, under different weak-beam diffracting conditions. A high density of dot-like debris accumulated at the interface with the Burgers vector pointing out of the interface is visible in figure 7 (*a*). The other

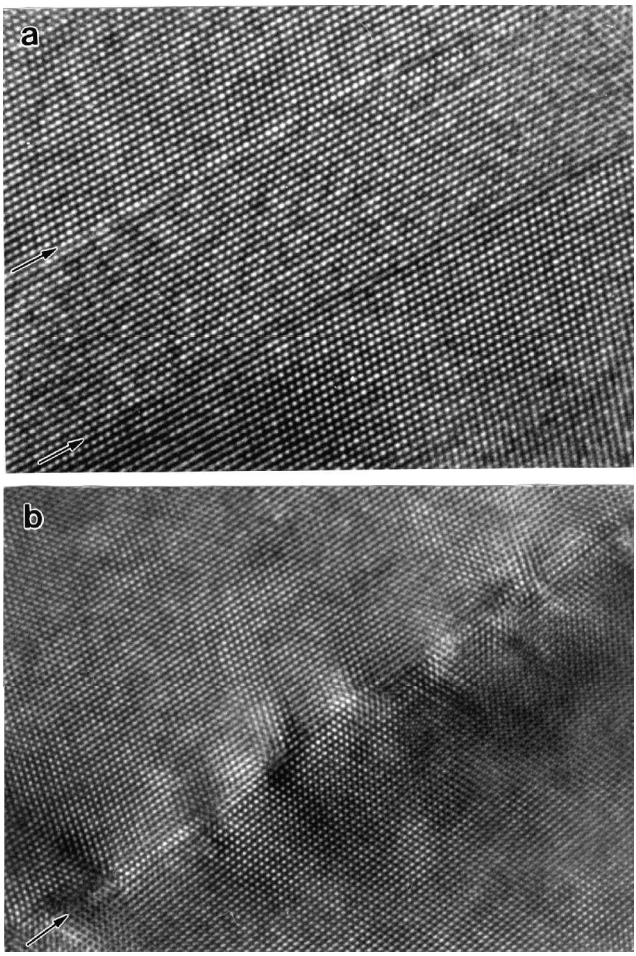

Figure 6. HREM observations of the layer-like structure at the beginning of region C, showing (*a*) the coherent matrix–twin boundary and (*b*) the accumulation of dislocations at the interface at the advanced region C. The arrows show the position of the matrix–twin interface.

interfacial dislocations are visible also in $\mathbf{g} = [0\bar{2}0]$ and $\mathbf{g} = [\bar{2}00]$ reflections in figures 7 (*b*) and (*c*) respectively. From both the weak-beam observations (figure 7) and the direct resolution micrographs (figure 6 (*b*)), one can estimate that the density of dislocations accumulated at the interface is of the order of $10^{16}\,\mathrm{m\,m^{-3}}$ at this stage of deformation. The weak-beam analysis shown in figure 7 indicates that there are a number of Burgers vectors present among the dislocations stored in the twin phase. The fine dot-like defects are distributed in the entire volume of the dislocated lattice, as shown in figure 7.

3.2.4. *Dislocation density measurements*

Efforts were undertaken to measure the dislocation density at large strains, based on the TEM two-beam and weak-beam micrographs. These results, as compared with the electrical resistivity measurements, are presented in table 1. The estimations

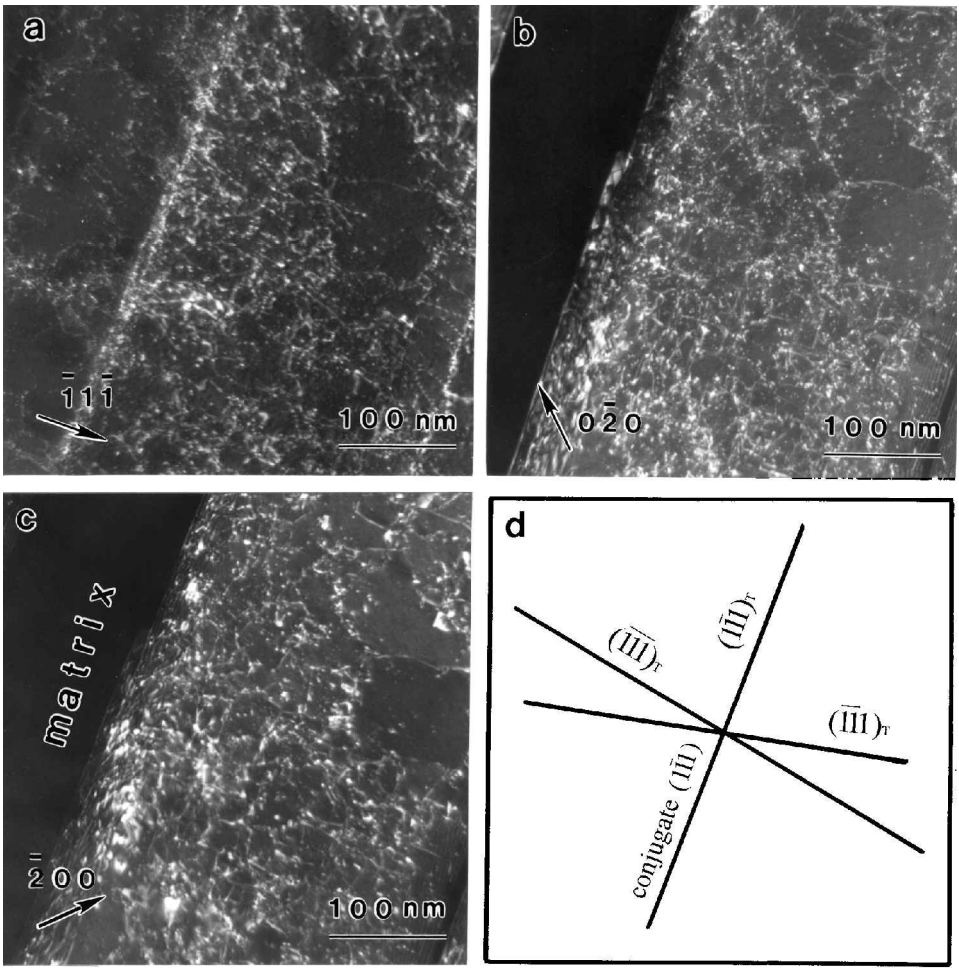

Figure 7. The dislocation substructure inside the twin phase at the end of the region C, where the observations were carried out in the foil parallel to the $(001)_T$ plane inside the twin corresponding to the initial $(1\bar{1}\bar{1})_M$ cross surface of the undeformed crystal: (*a*) debris accumulated on the interface with Burgers vector pointing out of the reflecting plane which is visible in $\mathbf{g} = [\bar{1}1\bar{1}]$; (*b*), (*c*) other interfacial dislocations which are visible in (*b*) $\mathbf{g} = [0\bar{2}0]$ and (*c*) $\mathbf{g} = [\bar{2}00]$; (*d*) traces of {111} planes on the observation plane. Note a very high density of fine dot-like defects distributed in the volume of the foil.

Table 1. Density of dislocations estimated from TEM two-beam and weak-beam micrographs compared with the electrical resistivity measurements. Dislocation densities were calculated from electrical resistivity data; the specific resistivity of dislocation was taken as $1 \times 10^{-25}\,\Omega\,m^3$ (Niewczas *et al.* 2001).

		Dislocation density ($10^{14}\,m\,m^{-3}$)		
Tensile stress (MPa)	Temperature (K)	Two-beam bright-field TEM	Weak-beam TEM	Resistivity measurements
400	4.2	3.4	9.6	16
460	4.2	4	11.3	20
540	4.2	4.3	16.3	25

of the dislocation density in the unit volume of the crystal, based on the weak-beam and two-beam observations, differ by a factor of two or three (table 1). The accuracy of dislocation density measurements based on TEM observations is low compared with the electrical resistivity measurements (table 1). This discrepancy can be attributed to the fine dot-like defects, which contribute to the resistivity, but are very difficult to count even under weak-beam diffracting conditions.

4.3. *Stability of dislocation debris against annealing at elevated temperatures*

Lattice dislocations are immobile between 4.2 and 300 K. Thus, it might be expected that the annealing of the deformed crystals at room temperature has a minimal influence on the dislocation substructure. In order to investigate these effects and in particular the effect of the temperature on the stability of the disloca-

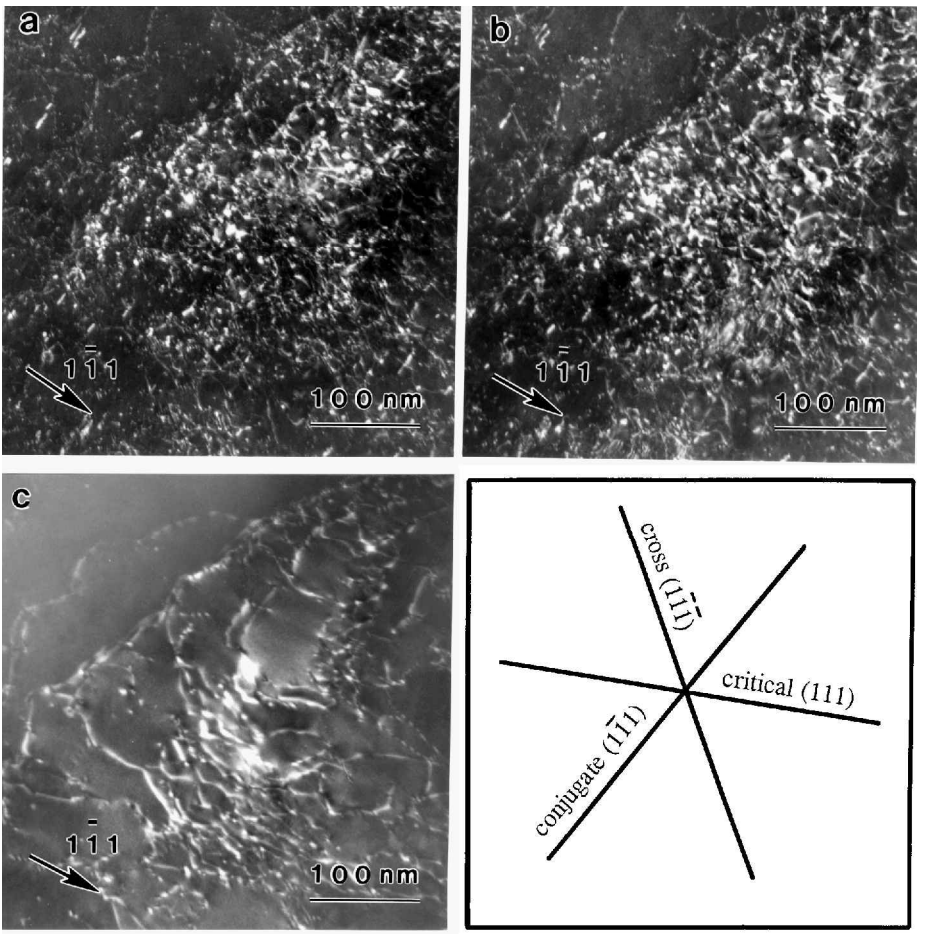

Figure 8. *In-situ* weak-beam observations of the dislocation substructure developed in crystal deformed up to twinning at 4.2 K during annealing at elevated temperatures, where the observations are carried out in the section parallel to the primary glide plane; (*a*) the initial structure, visible under weak-beam diffracting conditions at room temperature; (*b*), (*c*) the same area after annealing at (*b*) 373 K and (*c*) 573 K for 15 min; (*d*) traces of all {111} planes on the observation plane.

tion substructure developed at 4.2 K and observed under TEM, some specimens were annealed in the microscope at elevated temperatures and these results are shown in figure 8. Figure 8 (*a*) shows the structure of the parent crystal deformed up to the onset of twinning ($\sigma \approx 420$ MPa (figure 1)), observed in the section parallel to the primary glide plane $(11\bar{1})_M$. A high density of primary dislocations and short faulted dipoles aligned along the intersection of the primary and conjugate planes is visible in the structure in figure 8 (*a*). Annealing the thin foil at the temperature of 373 K for 15 min had almost no effect on the dislocation substructure, as shown in figure 8 (*b*). Further annealing at elevated temperatures is required to remove the short dipoles from the lattice and to rearrange the remaining dislocations by the climb. The substructure annealed at 573 K for 15 min clearly exhibits a polygonized arrangement as shown in figure 8 (*c*).

Resistivity data presented in part I (Niewczas *et al.* 2001), have shown that for Cu a large part of the deformation induced resistivity anneals out between 4.2 K and room temperature. In order to investigate whether this is general behaviour, the

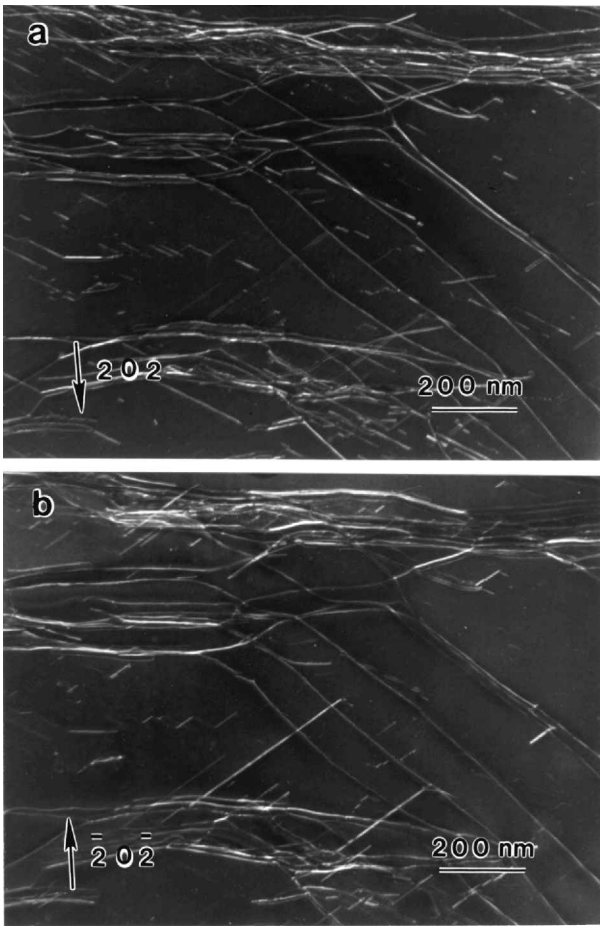

Figure 9. Weak-beam observations of the dislocation substructure in Cu–5 at.% Ni single crystals deformed to the resolved shear stress of 30 MPa (a tensile stress of 60 MPa) at 4.2 K: (*a*), (*b*) observations were carried out on the section parallel to the primary glide plane in $\mathbf{g} = \pm[202]$ reflections.

annihilation studies were carried out using [541] Cu–Ni single crystals deformed at 4.2 K (figure 1). The amount of deformation-induced resistivity that anneals out below room temperature was always lower in these alloys than in the pure Cu.

Cu–5 at.% Ni alloy crystals of stacking fault energy higher than Cu were chosen for the observation of the dislocation substructure. Figure 9 shows the dislocation substructure developed in this alloy after the deformation of 30 MPa of the resolved shear stress (a tensile stress of 60 MPa (figure 1)) at 4.2 K. The substructure was observed under TEM conditions within 12 h of an experiment at 4.2 K. The substructure exhibits very planar arrangements of long primary dipoles, a typical arrangement of dislocations observed in low-stacking-fault-energy alloys.

§4. Discussion

4.1. *Defect structure in deformed crystals*

Prior to discussing the substructure in deformed crystals it is germane to reiterate the observations concerning the character of the dislocation debris resulting from agglomeration of quenched-in vacancies in Cu crystals. The aggregation of quenched-in vacancies in the lattice produces spherical subnanometre vacancy clusters or sessile dislocation loops when the number of excess vacancies is very large. These defects lie on a variety of habit planes and thus are represented by a spectrum of Burgers vectors of the type $(a/3)\langle 111\rangle$. The fine-scale loop debris observed in the substructure of deformed crystals are consistent with the refinement of the dislocation dipoles produced by active dislocations and chopped by dislocations gliding in non-coplanar slip systems. The analysis of the nature of the fine dipole debris suggests that mechanisms other than the condensation of single vacancies or groups of vacancies into loop defects produce these defects. It is appropriate to consider whether the observed dipole debris can be related to the removable component of the electrical resistivity and this is addressed in §4.2.

During the region A, wherein the deformation proceeds primarily by the dislocation glide in the primary slip system (Niewczas *et al*. 2001), the substructure evolves into a complicated three-dimensional dislocation network. The primary dislocations are accumulated in layers parallel to the primary glide plane, but deviation up to about 10° in these dislocation layers from the exact crystallographic orientation of the primary slip plane is observed at larger deformations (figure 3). As the deformation proceeds, the dislocation substructure undergoes significant refinement by chopping of the dipoles due to the activity of the secondary glide (Basinski 1964, Fourie 1968). At higher strains in the region A the cell structure is formed, by the accumulation of secondary dislocations in the non-coplanar planes, differentiating regions of relatively low dislocation densities (cell interiors) from highly dislocated regions (dislocation walls). The average cell diameter at 4.2 K is of the order of 0.3–0.4 μm. Additionally, the weak-beam observations reveal fine dot-like defects. This structure is almost invisible under two-beam diffracting conditions, because it consists of short dislocation dipoles and loops of the size which is much below the extinction distance for typically operating strong beam reflection (Hirsch *et al*. 1977). The distortion of the lattice introduced by these defects is short range, therefore their displacement field cannot be analysed under strong beam diffraction conditions but can be probed by means of the weak-beam diffraction technique. The dot-like debris has been identified as short faulted dipoles of vacancy type. They are produced by the transformation of the primary unfaulted dipoles provided that the

primary dipoles are oriented along ⟨110⟩ direction and their height is lower than some critical value, usually less then 10 nm for Cu (Steeds 1967, Carter and Holmes 1975, Wintner and Karnthaller 1978). As the deformation proceeds, faulted dipoles are chopped into increasingly shorter lengths by the secondary slip as are the other elements of the dislocation substructure.

The nanoscale dipoles and loops derived from the operating dislocations can be easy distinguished from defects that are formed by the condensation of vacancies and are similar in appearance. The latter are randomly distributed on close-packed {111} planes and thus have random Burgers vector of $(a/3)\langle 111\rangle$ type, whereas the former defects have Burgers vectors derived from the dislocations activated during the deformation process as discussed above.

Twinning deformation occurs in crystals deformed at 4.2 K and converts about 70% of the parent crystal into twin-related orientation (Niewczas *et al.* 2001). The structure composed of layers of matrix and layers of twin develops new dislocation substructure during the subsequent co-deformation process in region C. TEM observations show that the average thickness of a homogeneous matrix and twin layers is about 50–100 nm. This is smaller than the average cell dimension developed in the parent crystal prior to twinning by a factor of almost ten and indicates that, in general, the twin width is not inherited from the scale of the cell structure of the parent crystal and that the dense dislocation network is penetrable by the twinning dislocations. The twinning must then transform the dislocation substructure of the parent crystal to the new configuration. This process involves both the transformation of the Burgers vector and the dislocation line and in the case of the transformation of primary dislocations it has been discussed previously by Basinski *et al.* (1997). The transformation of the other elements of the dislocation substructure will be considered elsewhere.

Primary dislocations and their derivatives, the main elements of the pre-existing dislocation substructure, act as forest dislocations for the operating twinning dislocations. The overall dislocation structure in the twinned crystal is further refined and therefore it is less stable against the anneal at temperatures higher than the deformation temperature. Chopped dislocation dipoles and small loops are now in close contact with effective sinks such as dense dislocation networks and the matrix–twin interfaces. The presence of these sinks affects the kinetics and the rate by which some part of the fine debris is removed from the substructure. The recoverable resistivity component in the twinned crystals is thus appreciably higher than in the matrix prior to twinning (Niewczas *et al.* 2001), because more debris can be removed by pipe diffusion to the sinks.

The matrix–twin interfaces introduced by twinning affect the subsequent deformation processes. The deformation after twinning proceeds at a very high hardening rate, because dislocations are accumulated on the scale of the matrix–twin interfaces which act as a hard impenetrable obstacles for glide dislocations. The interfaces are complex, because they contain much debris with a number of Burgers vectors, as was shown in figure 7. The analysis of the substructure from the region C is difficult because of high dislocation densities and the complex dislocation arrangement. TEM observations reveal very high densities of dot-like defects distributed in the entire volume of the crystal at this stage of deformation (figure 7). From their appearance they might be interpreted as vacancy clusters. However, a rough estimation of the density of these defects in the foil would give an overall concentration of vacancies in

the volume of the crystal, exceeding that at the melting point, which indicates that they are unlikely to be formed by the condensation of the deformation induced point defects. Moreover, analysis using the weak-beam diffraction technique indicates that some part of the present debris is inherited from the matrix substructure, whereas the others are derived from currently active dislocations.

4.2. *Thermal rearrangement of dislocations: annihilation of dipoles and loops*

In part I (Niewczas *et al*. 2001) it was shown that the major changes in the deformation-induced resistivity in Cu single crystals at 4.2 K occur because of heating to room temperature. The activation energy of the process was estimated to be of the order of 0.2–0.3 eV, suggesting that some defect species anneal by pipe diffusion or by volume diffusion as complex multivacancies. TEM studies of the dislocation substructure are subsequent to the changes in the overall defect structure and thus cannot provide information about defects that have annealed out previously. However, the recovery process proceeds continuously at elevated temperatures and thus TEM is useful to define the state of the recovered substructure. The *in-situ* observations carried out in the transmission electron microscope showed that no significant changes in the substructure occurs after annealing at 373 K. Defects that are removed were primarily narrow dislocation dipoles (figure 8 (*b*)). These observations agree well with the resistivity measurements carried out on bulk samples, which show only 10% change of recoverable resistivity after annealing for 50 h at 373 K relative to the resistivity which changes at room temperature. Annealing of this structure at temperatures up to 573 K causes polygonization (figure 8 (*c*)) and subsequent recrystallization, resulting in a rapid decrease in the electrical resistivity (Niewczas *et al*. 2001).

The dislocation dipoles and loops can be annealed out by continuous removal of single vacancies which can further diffuse along dislocations or possibly by multivacancies which can diffuse out through the bulk material. In either case the Burgers vector of the parent defects will be preserved. Thus, the character of the Burgers vector of shrinking dislocation loops and narrow vacancy dipoles remaining in the substructure will be inherited from the character of the Burgers vector of the parent defects. Such observations have been reported already in the literature during the deformation of Zn and MgO. In this case, short dipole loops have been shown to be formed by pipe diffusion from longer pinched-off dipoles when deformed Zn and MgO are annealed above the deformation temperature (Price 1960, Washburn *et al*. 1960, Breghezan *et al*. 1961, Kroupa and Price 1961, Groves and Kelly 1962).

Pipe diffusion can be poisoned by impurity or alloying, and this may explain the fact that both the resistivity changes and the dislocation substructure changes in annealed crystals of Cu–5 at.% Ni at 295 K are smaller than in Cu crystals.

There is a disagreement between the dislocation density estimated from TEM observations compared with the electrical resistivity measurements (table 1). The accuracy in the determination of the dislocation density can be improved by using a weak-beam rather than the two-beam diffraction technique. However, the discrepancy between the weak-beam TEM and the resistivity method is still a factor of two. The inhomogenity of the substructure, some loss of defects during the preparation and difficulties in counting very fine loops may contribute to this discrepancy.

It is appropriate to consider that the observed dislocation density of $10^{16}\,\mathrm{m\,m^{-3}}$ at the end of deformation process must be close to the maximum attainable dislocation density in the crystalline material. The flow stress of the crystals at the point of

fracture is of the order of $\mu/100$, within a factor two or three of the theoretical strength. Thus, although it is a somewhat speculative view it is a possible that the density of defects at the twin–parent interface reaches a limit where local rearrangement in the absence of thermally activated events at 4.2 K can trigger the observed shear instabilities discussed in part I, as the crystal approaches failure.

4.3. *Production of point defects*

The current TEM results and the electrical resistivity results discussed in part I (Niewczas *et al.* 2001) suggest that some tentative conclusions can be drawn regarding the production of point defects during plastic deformation. It is often believed that both interstitials and vacancies can be produced by plastic flow. The migration energy of interstitials in Cu is of the order of 0.1 eV (Thompson 1969). Thus, if interstitials were present in the structure, they would be annealed out below 50 K and this would be manifested by a rapid increase in the electrical conductivity of the material (Thompson 1969). In the present experiments, there was no change in the electrical resistivity observed below 77 K, indicating that there are no interstitial point defects produced during plastic flow in Cu crystals at 4.2 K. This conclusion is in agreement with some previous results obtained by hyperfine spectroscopy methods (Collins *et al.* 1981, Petry *et al.* 1983) and electrical resistivity (Blewitt *et al.* 1955, Basinski and Saimoto 1967, Basinski and Basinski 1989), which also showed no evidence of the production of interstitials during plastic deformation in different materials.

The electrical resistivity results (Niewczas *et al.* 2001) show that some defect species anneal out from the structure between 77 and 250 K. The estimated migration energy of these defects is thus much below the migration energy for single vacancies in bulk diffusion, which is of the order of 0.7–0.8 eV. This difference and the current more direct TEM observations revealing the origin of fine dislocation debris suggest that single vacancies do not contribute to the recoverable component of the electrical resistivity and their production is appreciably suppressed. This conclusion may be supported by independent studies of the types of defect produced during the deformation of different materials by positron annihilation (e.g. Ni–20 at.% Co alloy by Adamenko *et al.* (1968), Cu and Al by Grosskreutz and Millett (1969) and Al by Hautojärvi *et al.* (1970)). The results presented by these researchers also show no evidence of vacancy production during the deformation in these materials.

The current study suggests that the annealing of the fine-scale dipole debris occurs by short-circuit diffusion of these defects to the present sinks such as dense dislocation network (e.g. cell walls) or parent–twin interfaces. This is consistent with both the estimated low migration energy of diffusing species and the extent to which annealable defects are produced and removed from the substructure during the region A of deformation (before twinning) and later during the region C (compatible co-deformation of the parent and twin phases). However, it is also possible that dipole debris anneal out (shrink) by the motion of some form of multivacancies diffusing through the lattice, which may also explain the resistivity data presented in part I.

§ 5. Conclusions

It is shown that fine dislocation debris is a prominent element of the defect structure in Cu crystals deformed at 4.2 K. These defects are identified as narrow faulted dipoles of vacancy type. They are produced at all stages of the deformation and are important components of dislocation walls and dense dislocation tangles.

Twinning, which occurs at advanced deformation, transforms the pre-existing dislocation substructure of the parent crystal to its new configuration inside the twin. During this process a significant refinement of the substructure takes place; refined defects are less stable against annealing and contribute more to the recoverable portion of the electrical resistivity. Processes with short-circuit diffusion must control the annealing of this debris. In Cu–5 at.% Ni crystals where the presence of an alloying element is expected to poison the pipe diffusion, the recoverable component of electrical resistivity is smaller. Twinning also has an important effect on the mechanical properties of the system. It introduces a high density of matrix–twin interfaces, which act as strong obstacles for dislocation glide, so the flow stress increases. These interfaces also provide new sinks for diffusing species. The present TEM observation shows that matrix–twin interfaces accumulate high dislocation densities during the co-deformation process in region C. Thus, it is possible that the final shear instability is initiated at places where the dislocation densities approach theoretical limits.

Acknowledgement

The financial support of Natural Sciences and Engineering Research Council (Canada) is gratefully acknowledged.

References

Adamenko, A. A., Dekhtyar, I. J., and Mikhalenkov, V. S., 1968, *Phys. Lett.* A, **26**, 288.
Antonopoulos, J. G., Brown, L.M., and Winter, A. T., 1976, *Phil. Mag.*, **34**, 549.
Antonopoulos, J. G., and Winter, A. T., 1976, *Phil. Mag.*, **33**, 87.
Basinski, Z. S., 1964, *Discuss. Faraday Soc.*, **38**, 93.
Basinski, Z. S., and Basinski, S. J., 1989, *Acta metall.*, **12**, 3275.
Basinski, Z. S., and Saimoto, S., 1967, *Can. J. Phys.*, **45**, 1161.
Basinski, Z. S., Szczerba, M. S., Niewczas, M., Embury, J. D., and Basinski, S. J., 1997, *Rev. Métall.* **94**, 1037.
Blewitt, T. H., Coltman, R. R., and Redman, J. K.,1955, *Proceedings of the Conference on Defects in Crystalline Solids*, Bristol, 1954 (London: Physical Society), p. 369.
Breghezan, A., Fordeux, A., and Amelinckx, S., 1961, *Acta metall.*, **9**, 464.
Carter, C. B., and Holmes, S. M., 1975, *Phil. Mag.*, **32**, 599.
Cockayne, D. J. H., Ray, I. L. F., and Whelan, M. J., 1969, *Phil. Mag.*, **20**, 1265.
Collins, G. S., Stern, G. P., and Hohenemser, C., 1981, *Phys. Lett.* A, **84**, 289.
Fourie, J. T., 1968, *Phil. Mag.* **17**, 735.
Grosskreutz, J. C., and Millett, W. E., 1969, *Phys. Lett.* A, **28**, 621.
Groves, G. W., and Kelly, A., 1962, *J. appl. Phys. Suppl.*, **33**, 456.
Hautojärvi, P., Tamminen, A., and Jauho, P., 1970, *Phys. Rev. Lett.*, **24**, 459.
Hirsch, P. B., Howie, A., Pashley, D. W., Nicholson, R. B., and Whelan, M. J., 1977, *Electron Microscopy of Thin Crystals* (Malabar, Florida: Robert E. Krieger).
Kroupa, F., and Price, P. B., 1961, *Phil. Mag.*, **6**, 243.
Mitchell, J. W., Chevrier, J. C., Hockey, B. J., and Managhan, J. P., 1967, *Can. J. Phys.*, **45**, 453.
Niewczas, M., Basinski, Z. S., Basinsky, S. J., and Embury, J. D., 2001, *Phil. Mag.*, **81**, 1121.
Petry, W., Brussler, M., Groger, V., Muller, H. G., and Vogl, G., 1983, *Hyperfine Interact*, **15–16**, 371.
Price, P. B., 1960, *Phil. Mag.*, **5**, 449.
Steeds, J. W., 1966, *Proc. R. Soc.* A, **292**, 343; 1967, *Phil. Mag.*, **16**, 771.
Thompson, M. W., 1969, *Defects and Radiation Damage in Metals* (Cambridge University Press), pp. 257–315.
Washburn, J., Groves, G. W., Kelly, A., and Williamson, G. K., 1960, *Phil. Mag.*, **5**, 991.
Wintner, E., and Karnthaler, H. P., 1978, *Acta metall.*, **26**, 941.